Electronic Supplementary Information

for the manuscript

Detection of Al^{3+} and Fe^{3+} ions by nitrobenzoxadiazole bearing pyridine-2,6-dicarboxamiade based chemosensors: Effect of solvents on detection

Sudheer,[†] Vijay Kumar,[†] Pramod Kumar and Rajeev Gupta*

Department of Chemistry, University of Delhi, New Delhi 110007, India

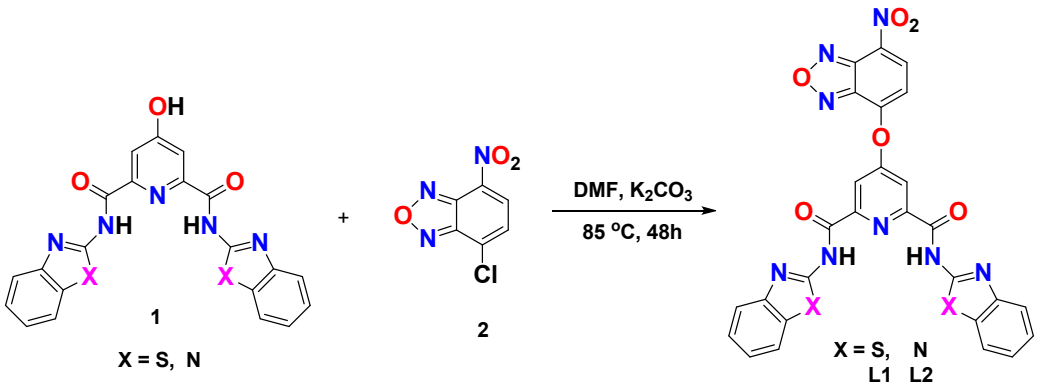

Scheme S1. Preparative route for the synthesis of chemosesnsors **L1** and **L2**.

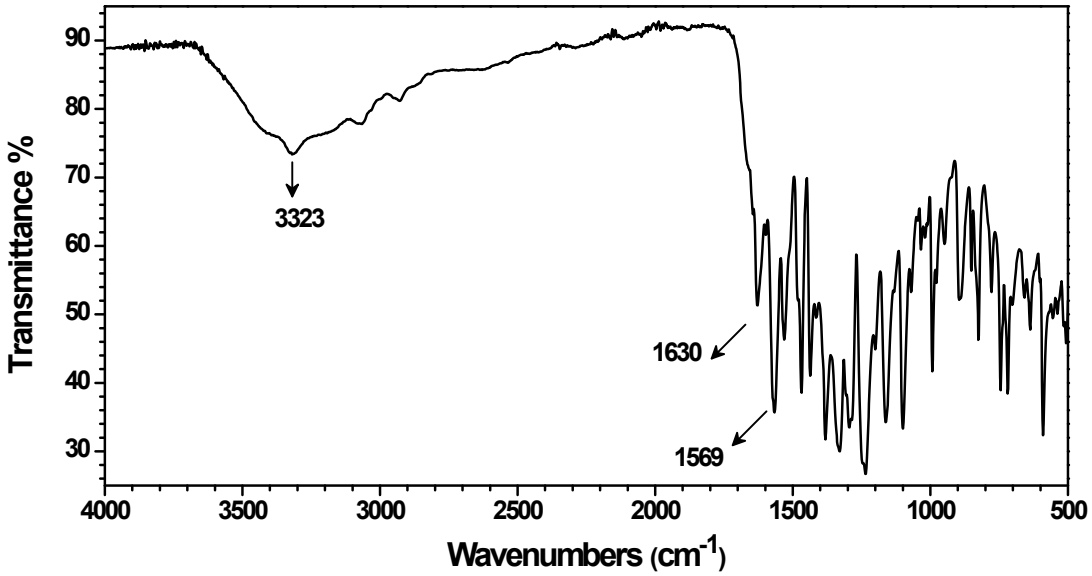

Figure S1. FTIR spectrum of chemosensor **L1.**

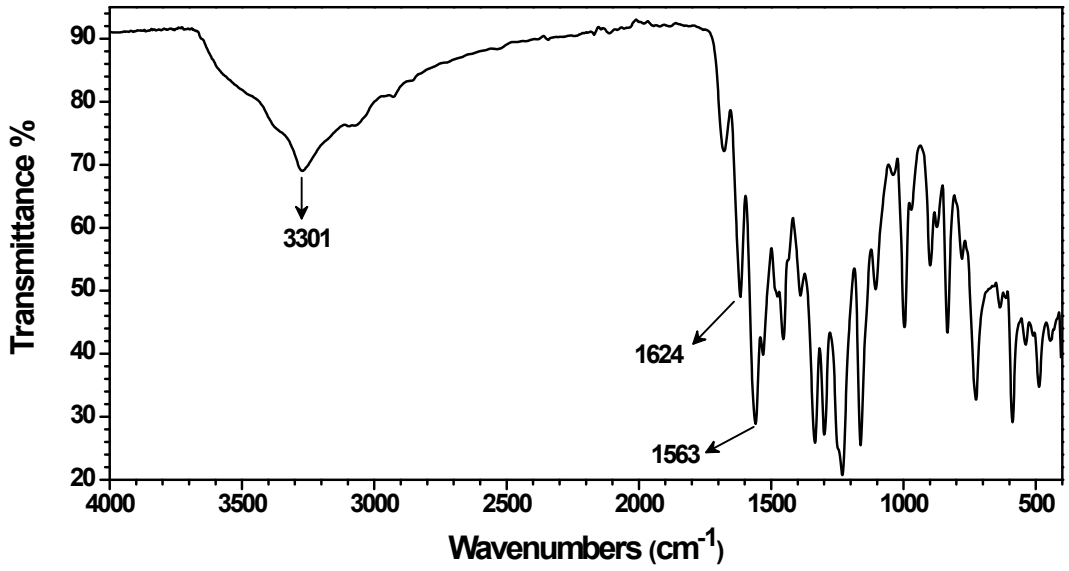

Figure S2. FTIR spectrum of chemosensor **L2.**

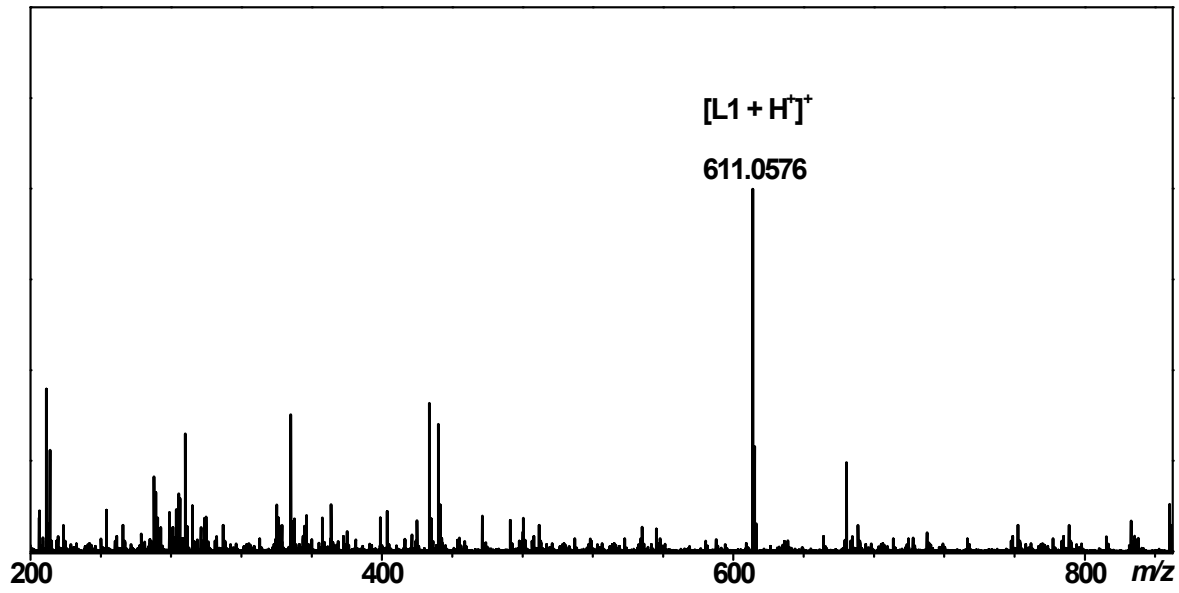

Figure S3. ESI$^+$-MS spectrum of chemosensor **L1** recorded in MeOH.

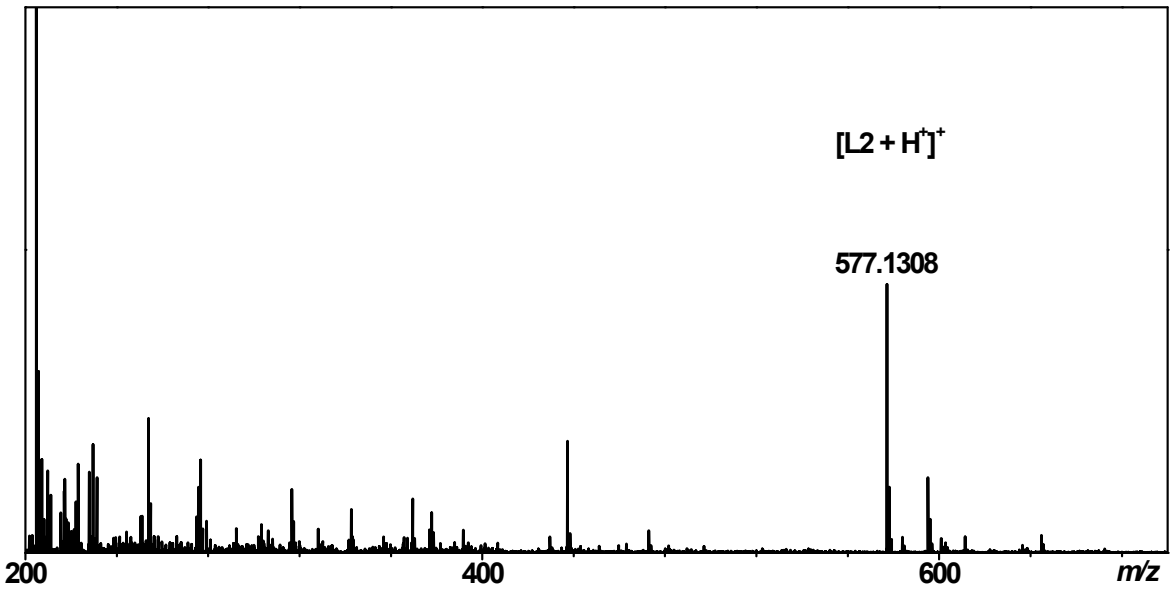

Figure S4. ESI$^+$-MS spectrum of chemosensor **L2** recorded in MeOH.

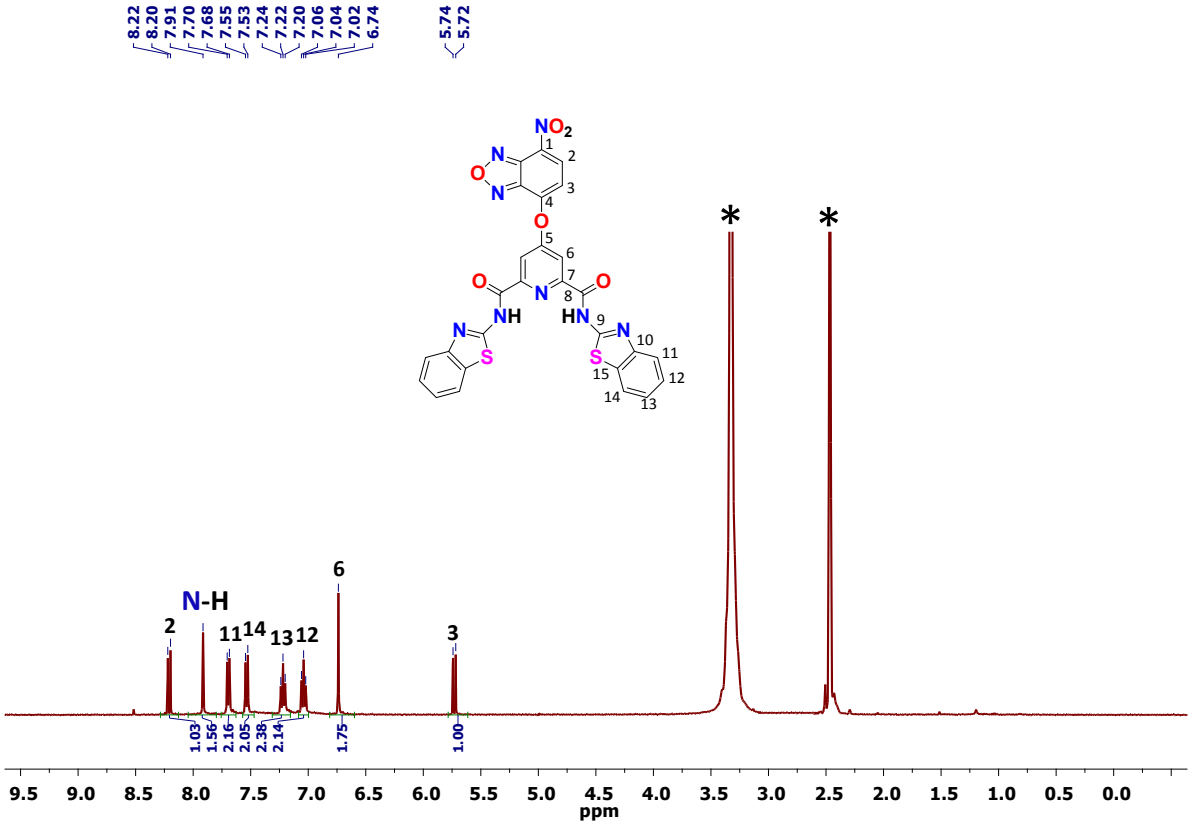

Figure S5. ^{1}H NMR spectrum of chemosensor **L1** recorded in DMSO-d_6.

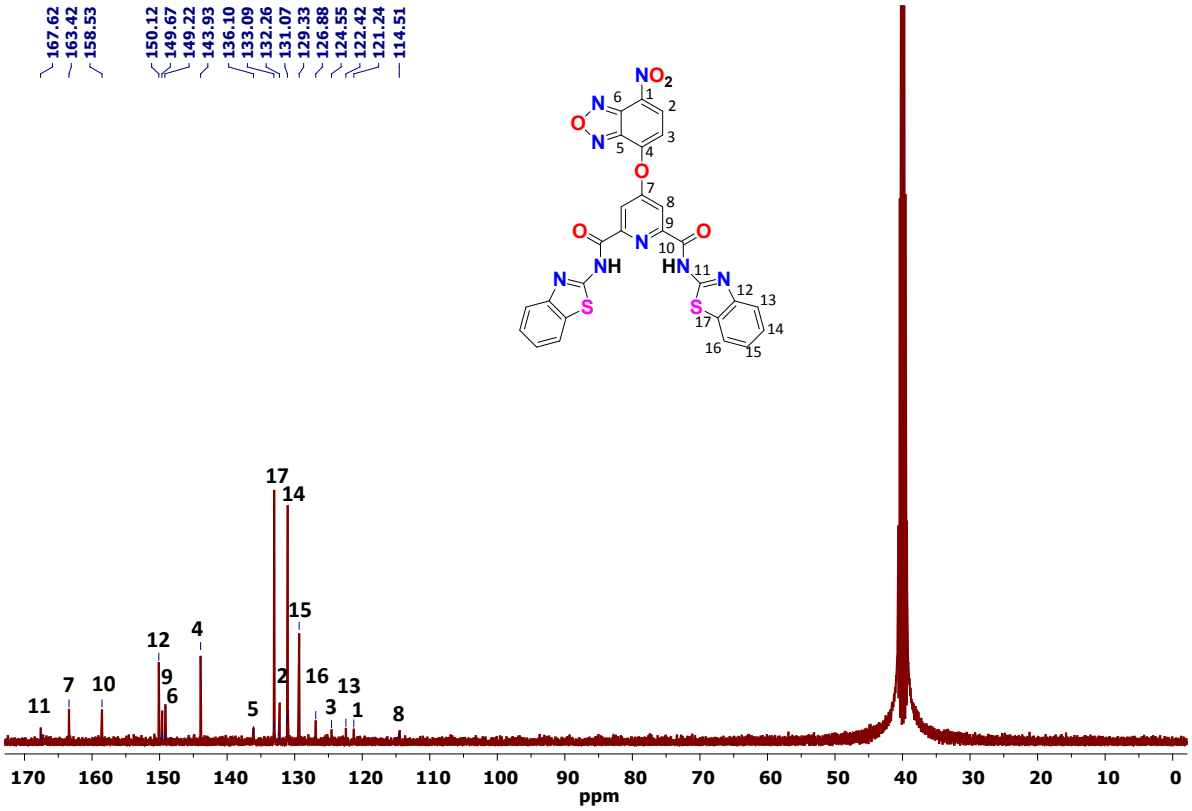

Figure S6. ^{13}C NMR spectrum of chemosensor **L1** recorded in DMSO-d_6.

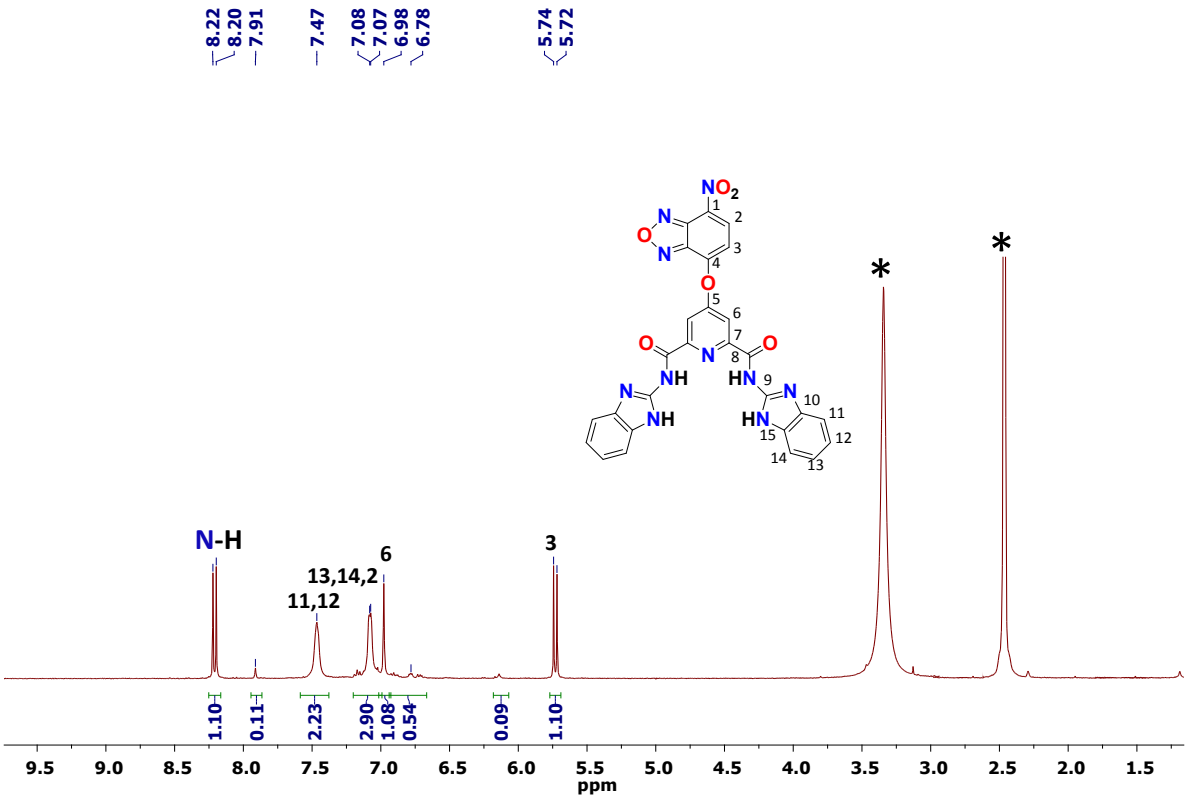

Figure S7. ^{1}H NMR spectrum of chemosensor **L2** recorded in DMSO-d_6.

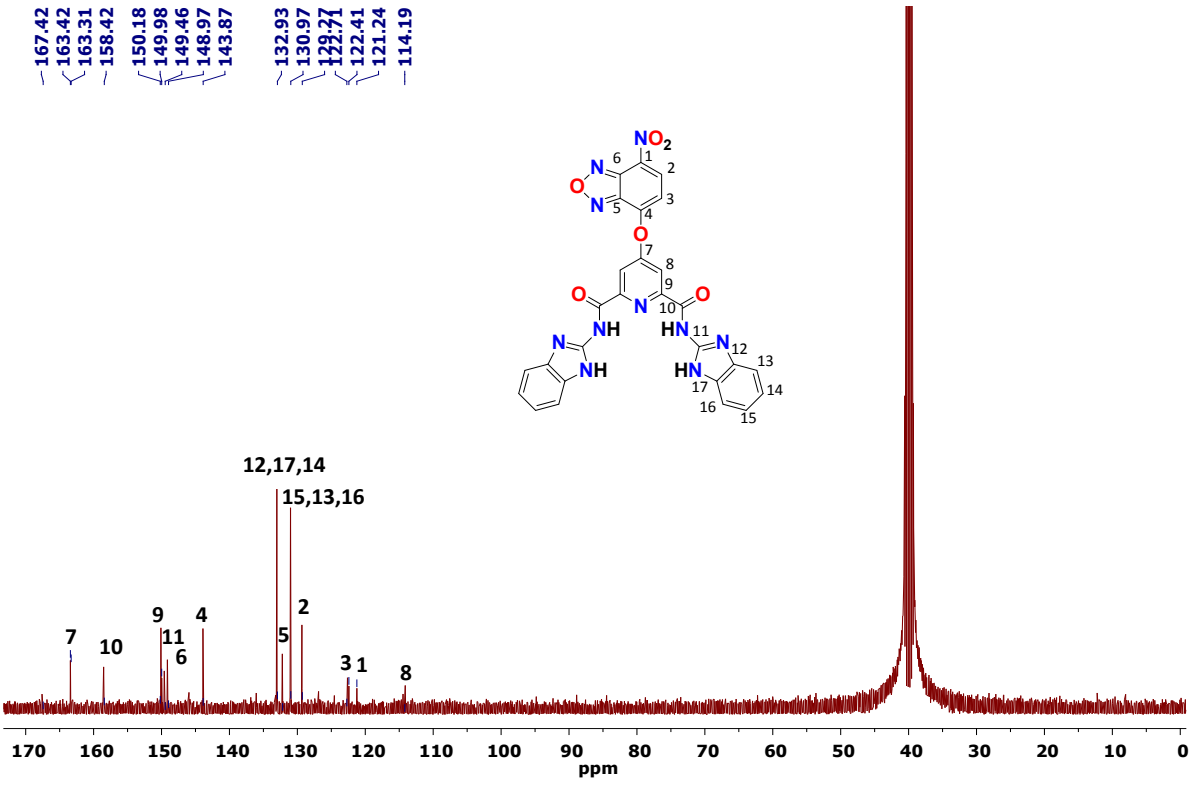

Figure S8. ^{13}C NMR spectrum of chemosensor **L2** recorded in DMSO-d_6.

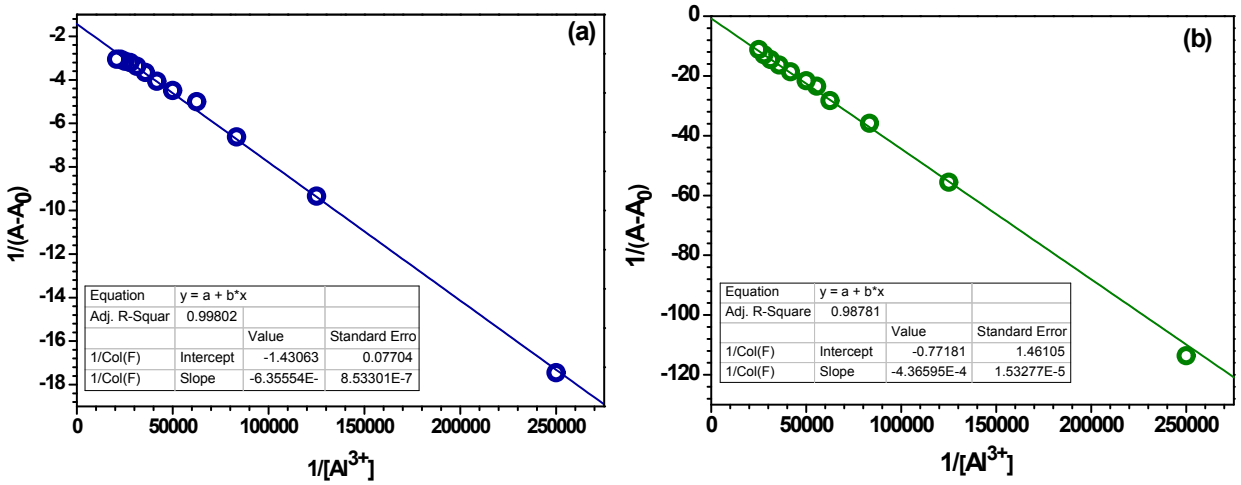

Figure S9. B-H plots by the absorption spectral titration for the detection of Al^{3+} ion by chemosensors (a) **L1** and (b) **L2** in CH_3OH.

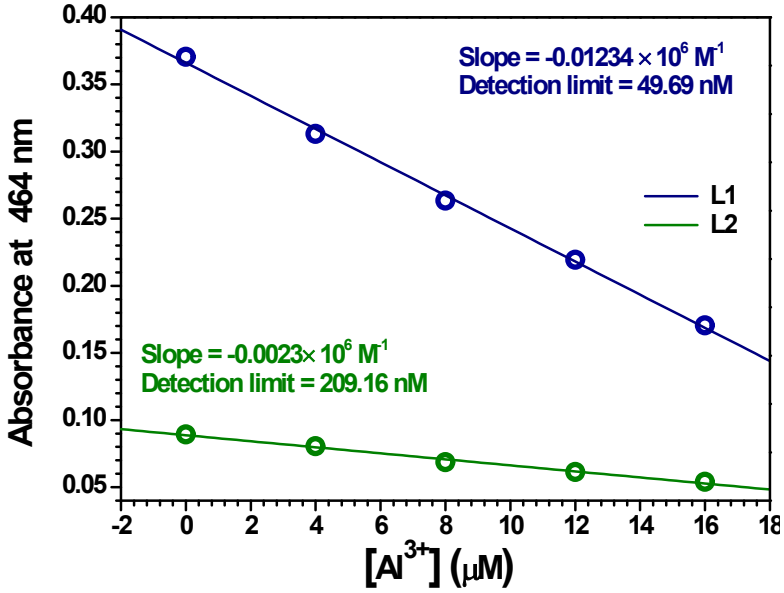

Figure S10. Determination of detection limits by the absorption spectral titration for the detection of Al^{3+} ion by chemosensors **L1** and **L2** in CH_3OH.

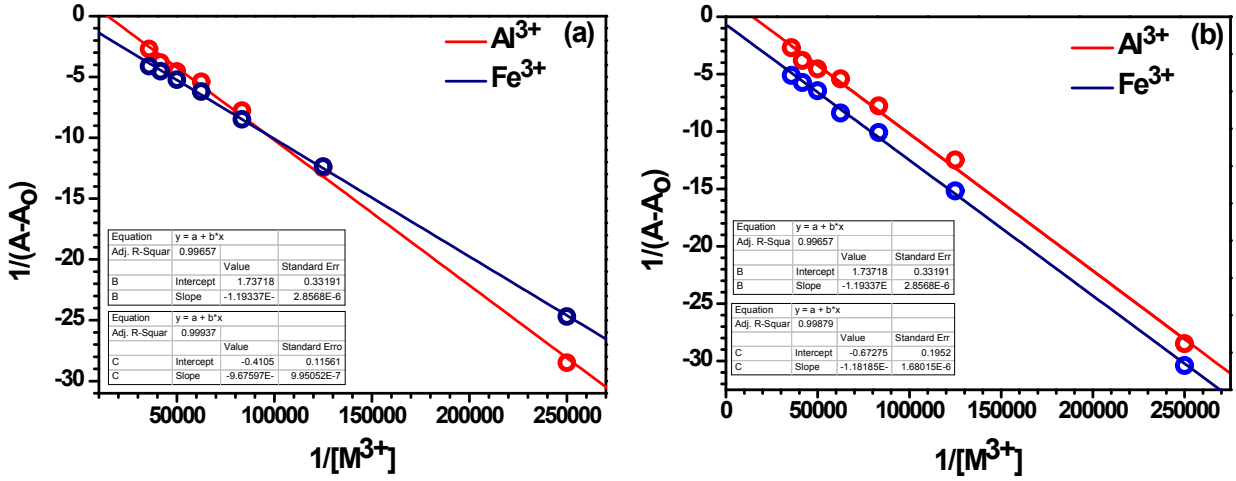

Figure S11. B-H plots by the absorption spectral titration for the detection of Al^{3+} and Fe^{3+} ions by chemosensors (a) **L1** and (b) **L2** in THF.

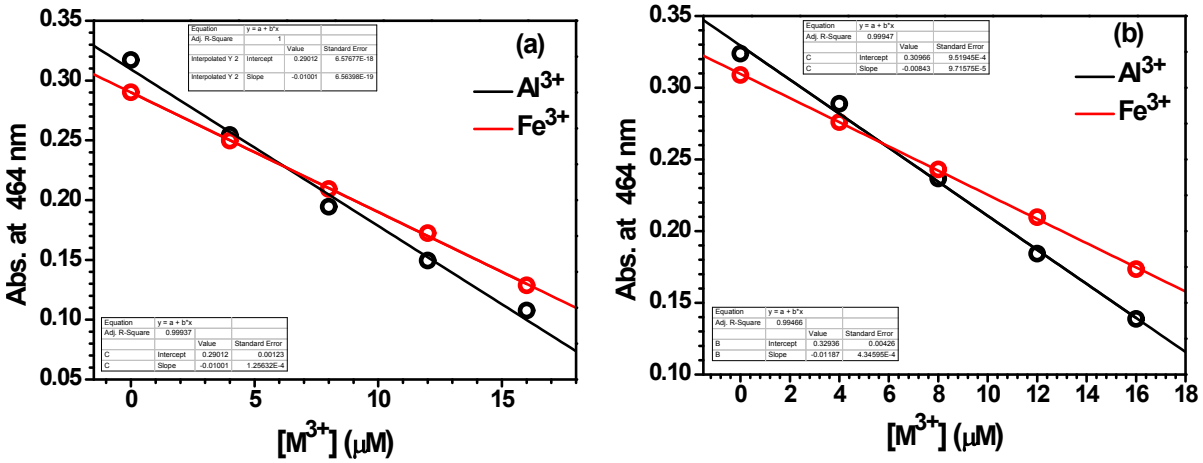

Figure S12. Determination of detection limits by the absorption spectral titration for the detection of Al^{3+} and Fe^{3+} ions by chemosensor **L1** and **L2** in THF.

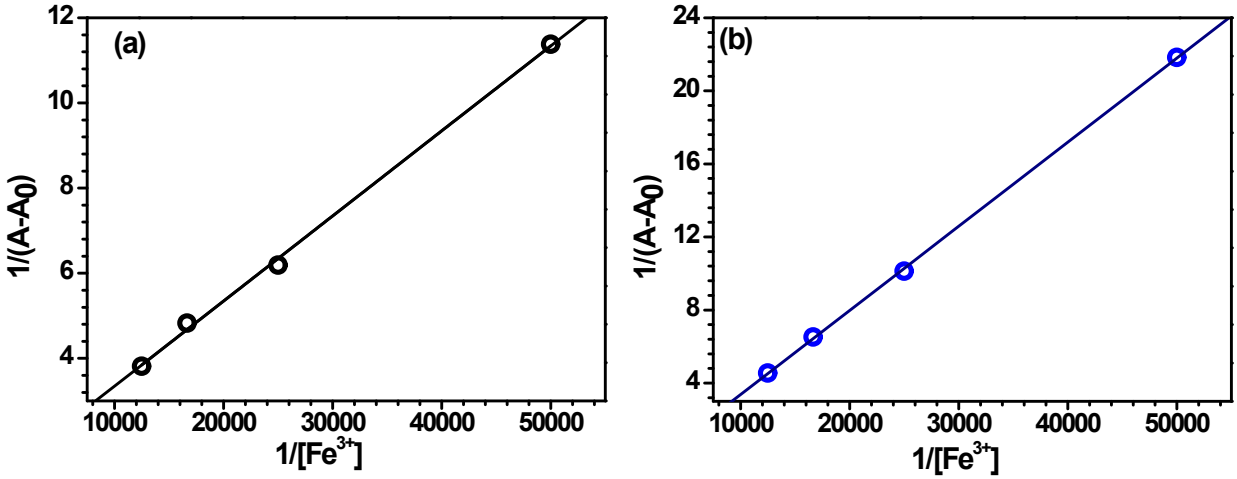

Figure S13. B-H plots by the absorption spectral titration for the detection of Fe^{3+} ion by chemosensors (a) **L1** and (b) **L2** in HEPES buffer (10 mM, pH = 7.2).

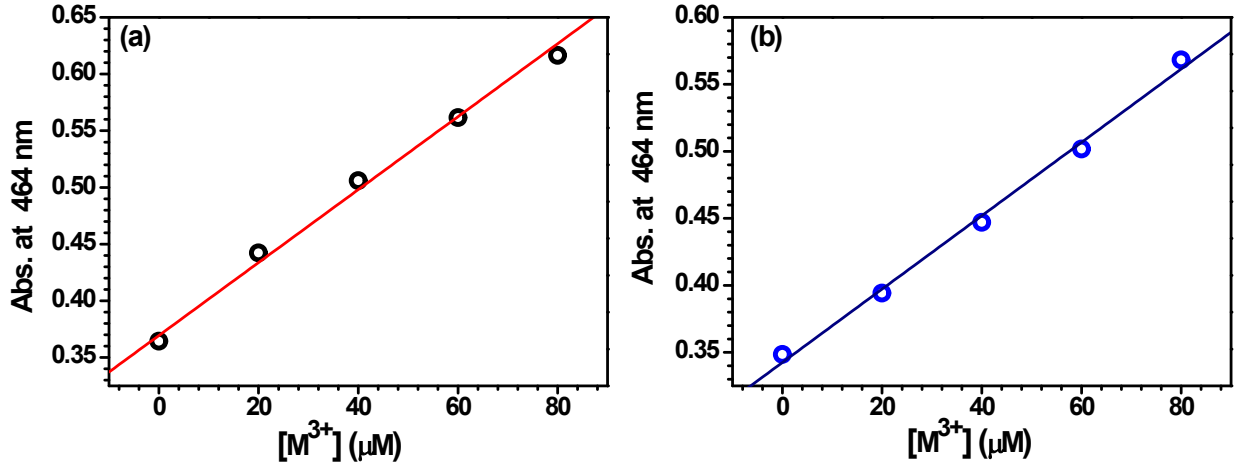

Figure S14. Determination of detection limits by the absorption spectral titration for the detection of Fe^{3+} ion by chemosensor **L1** and **L2** in HEPES buffer (10 mM, pH = 7.2).

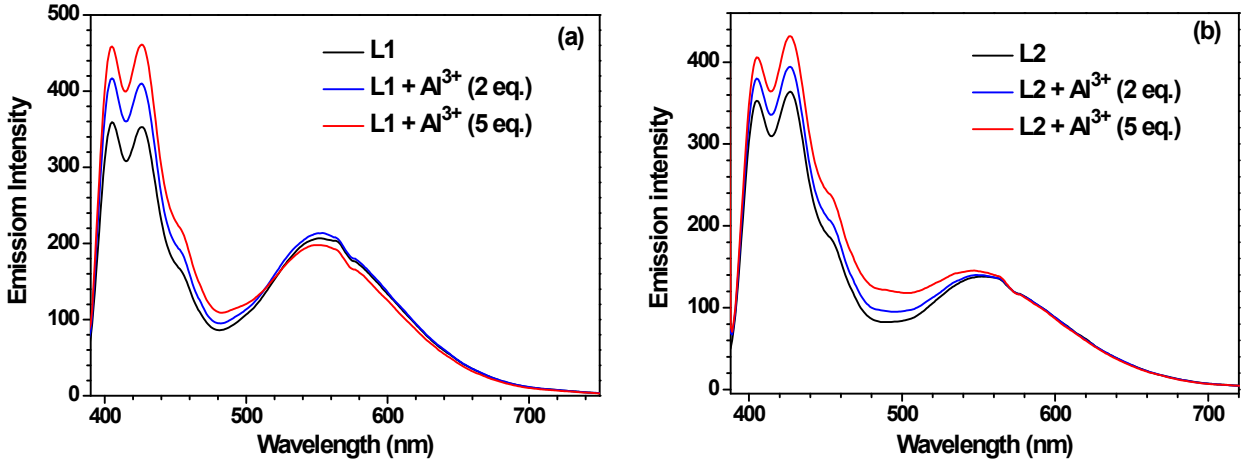

Figure S15. Change in the emission intensity with the number of equivalents (0–5 equivalents) of Al^{3+} ion for the chemosensors (a) **L1** (b) **L2** in CH_3OH.

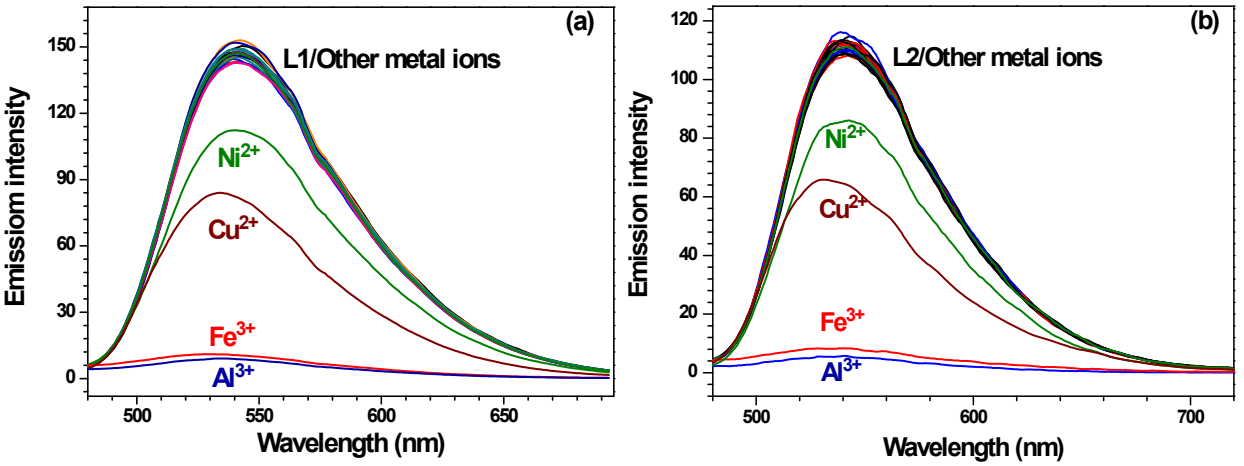

Figure S16. Change in the emission intensity of chemosensors (a) **L1** (20 μM) and (b) **L2** (20 μM) with 2 equivalents of assorted metal ions in THF.

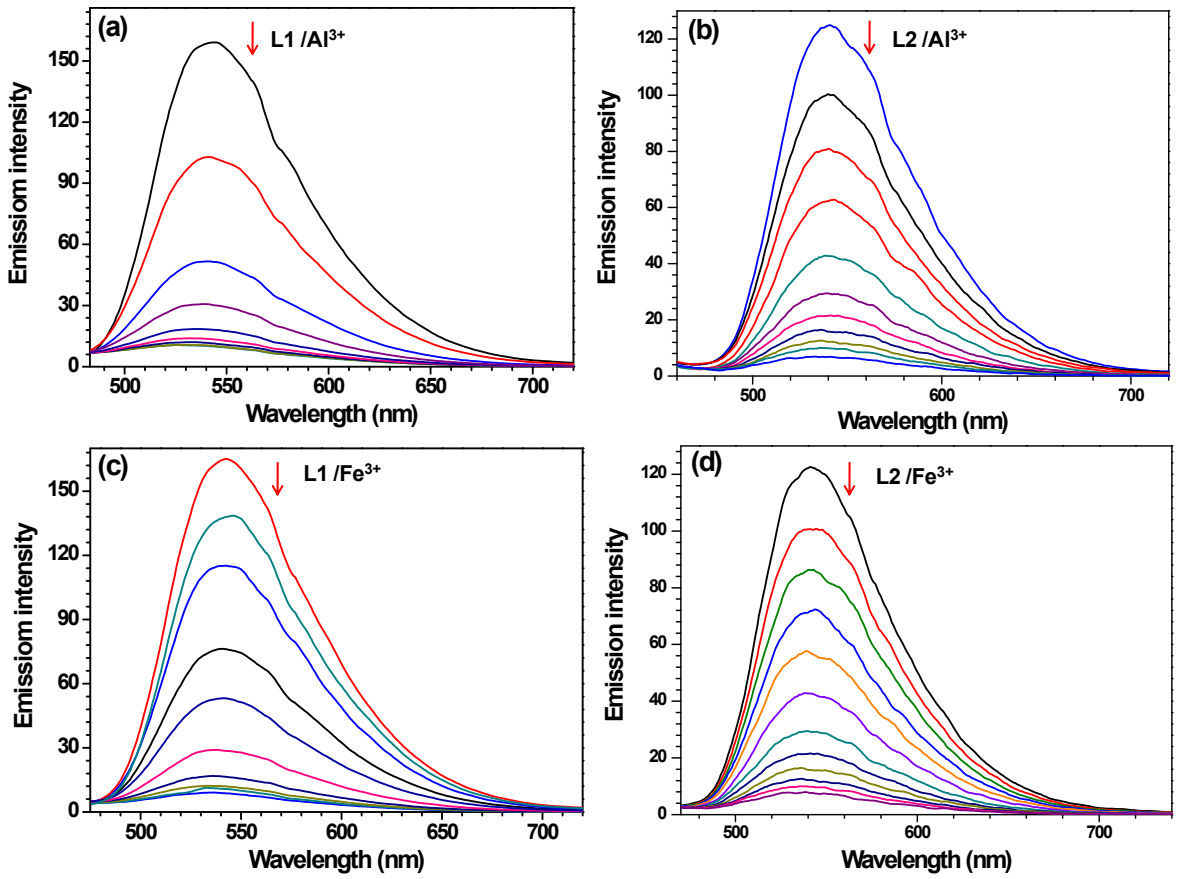

Figure S17. Change in the emission spectra of chemosensors **L1** and **L2** in THF: (a) **L1** (20 μM) with Al^{3+} ion (0-40μM); (b) **L2** (20 μM) with Al^{3+} ion (0-40μM); (c) **L1** (20 μM) with Fe^{3+} ion (0-40μM); (d) **L2** (20 μM) with Fe^{3+} ion (0-40μM).

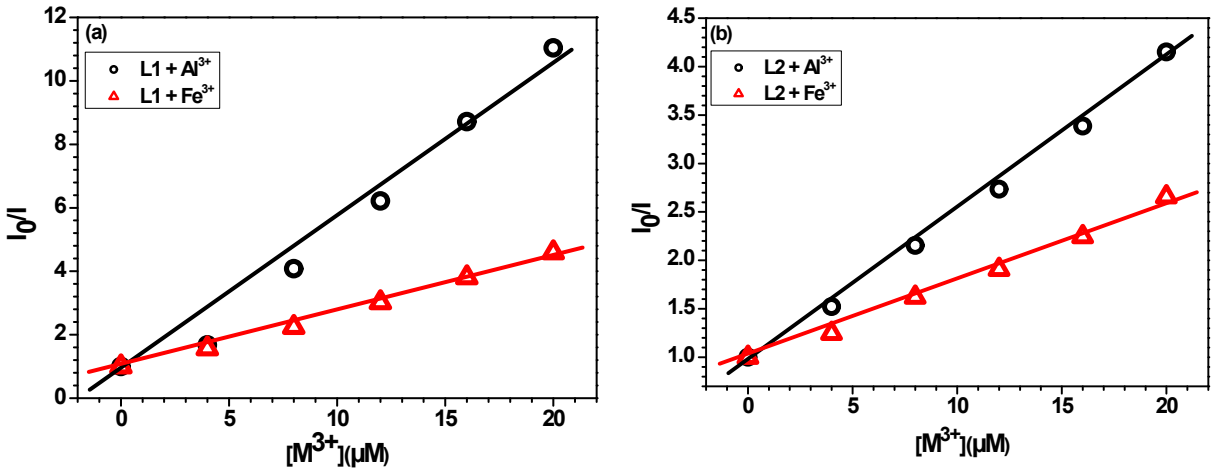

Figure S18. Stern-Volmer plots by the emission spectral titration for the detection of Al^{3+} and Fe^{3+} ions by the chemosensors (a) **L1** and (b) **L2** in THF.

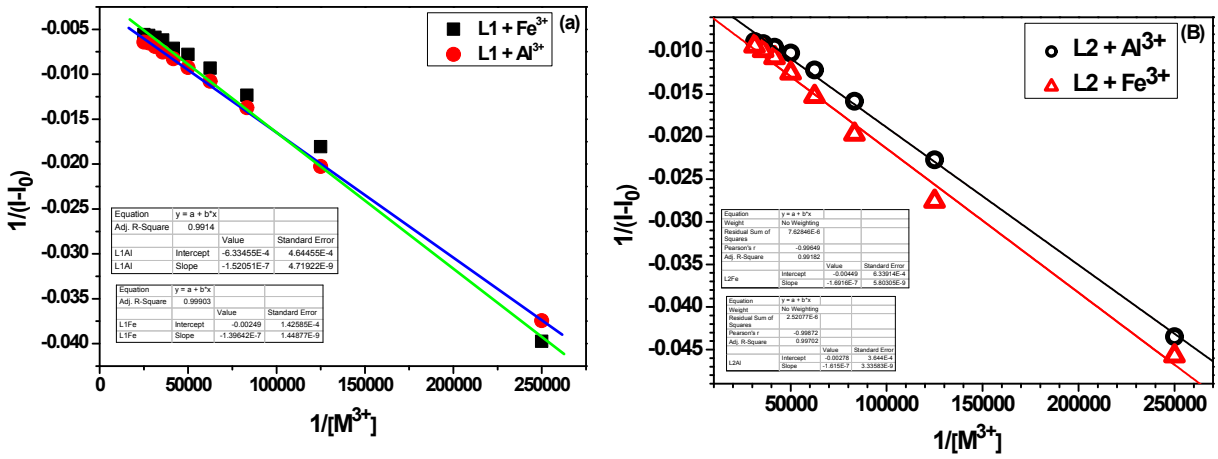

Figure S19. B-H plots by the emission spectral titration for the detection of Al^{3+} and Fe^{3+} ions by the chemosensors (a) **L1** and (b) **L2** in THF.

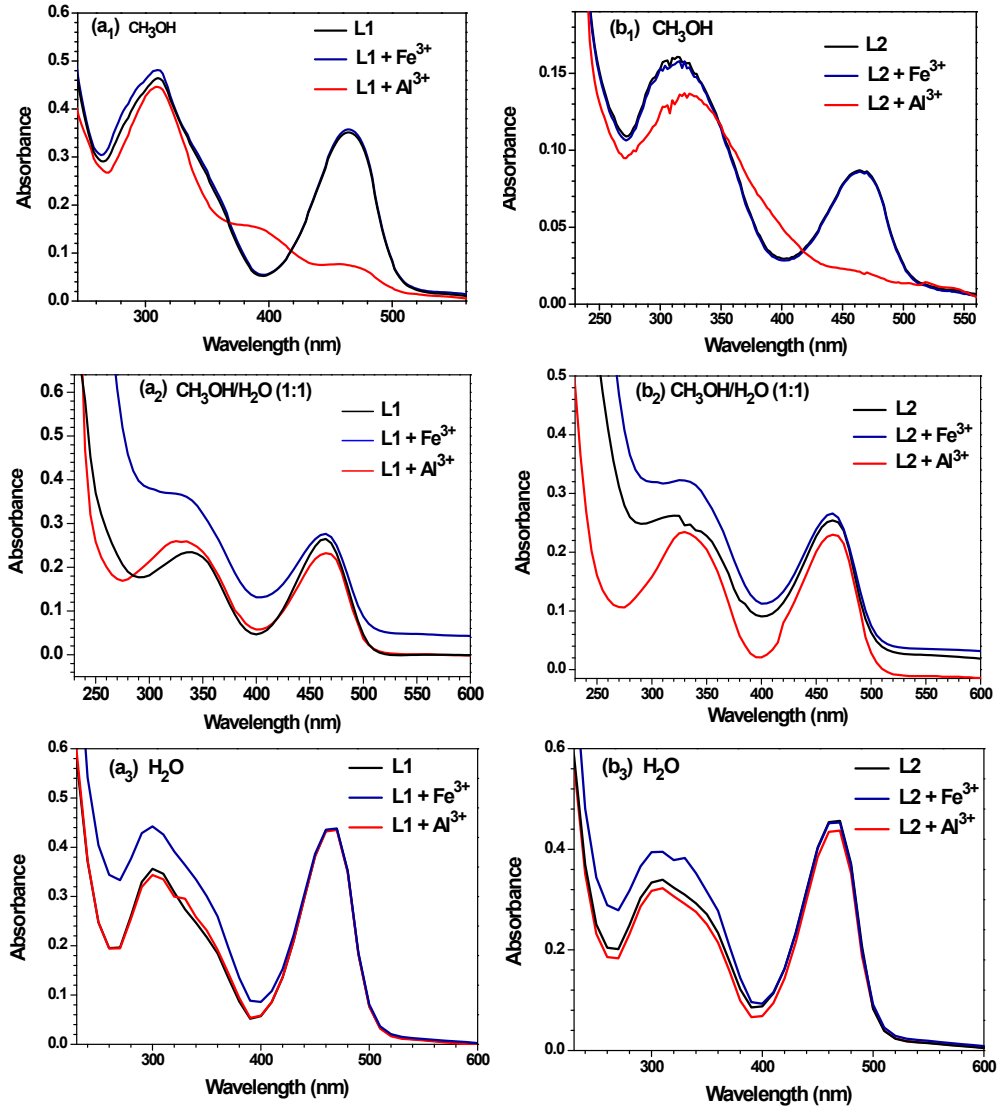

Figure S20. Change in the absorption spectra of chemosensors (a_1-a_3) **L1** and (b_1-b_3) **L2** in different CH_3OH–H_2O combinations (100%, 50% and 0%) with Al^{3+} and Fe^{3+} ions.

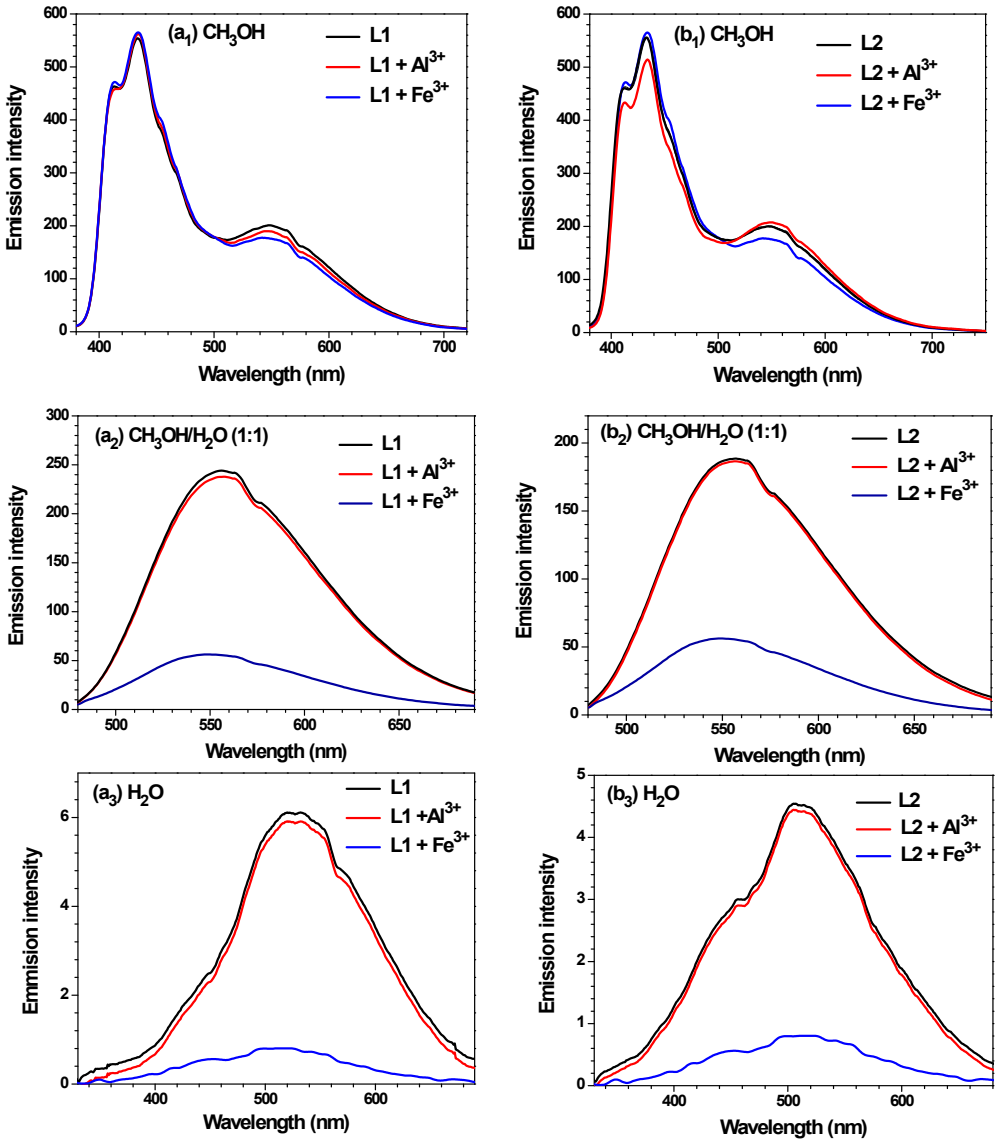

Figure S21. Change in the emission spectra of chemosensors (a_1-a_3) **L1** and (b_1-b_3) **L2** in different CH_3OH–H_2O combinations (100%, 50% and 0%) with Al^{3+} and Fe^{3+} ions. λ_{ex}= 370 nm in CH_3OH; λ_{ex}= 360 nm in CH_3OH–H_2O (1:1, v/v); λ_{ex}= 360 nm in H_2O.

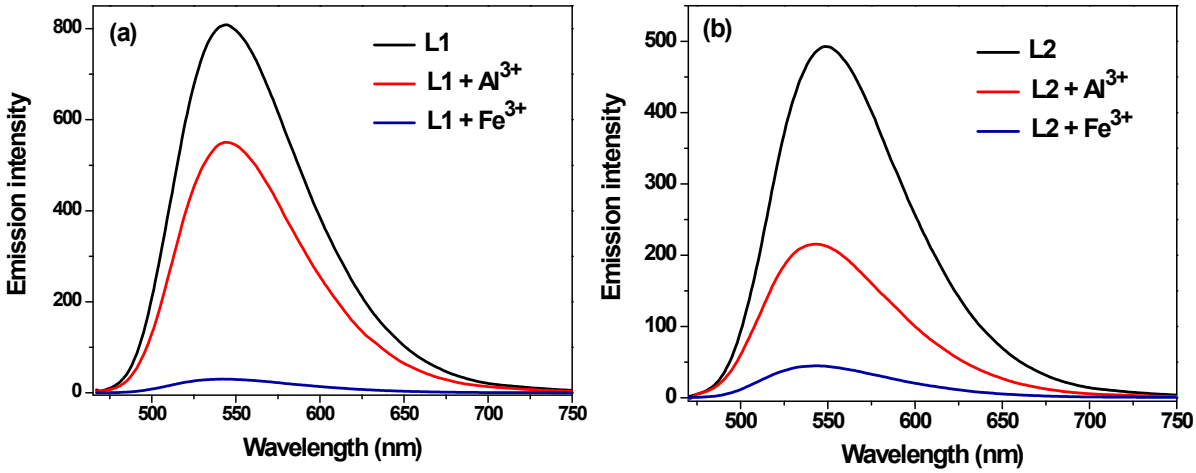

Figure S22. Change in the emission spectra of chemosensors (a) **L1** and (b) **L2** in the presence of Al^{3+} and Fe^{3+} ions in CH_3CN (λ_{ex} = 450 nm).

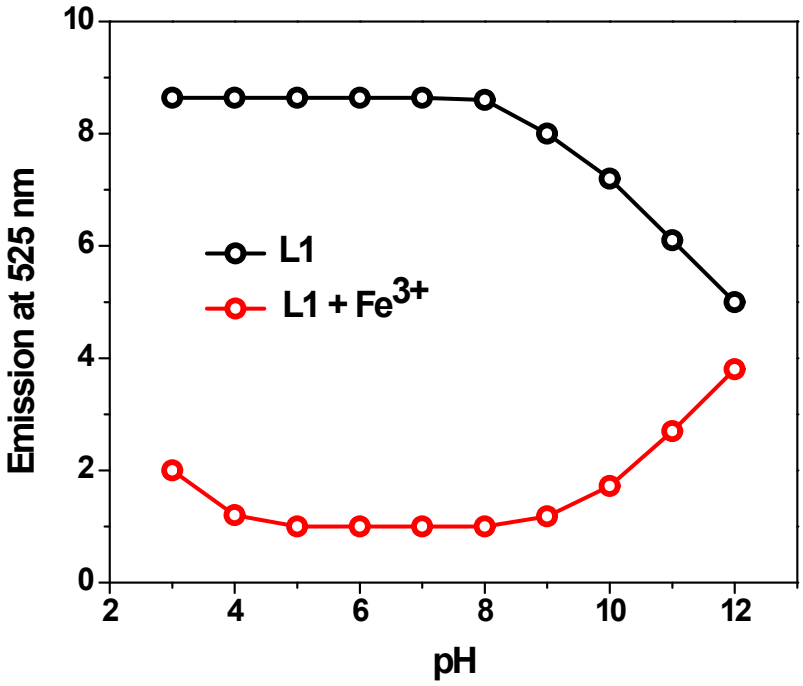

Figure S23. Effect of pH (3.0–12.0) on the emission intensity of chemosensor **L1** at 525 nm in the aqueous medium. The black and red circles respectively display emission intensity of chemosensor **L1** in the absence and presence of Fe^{3+} ion.

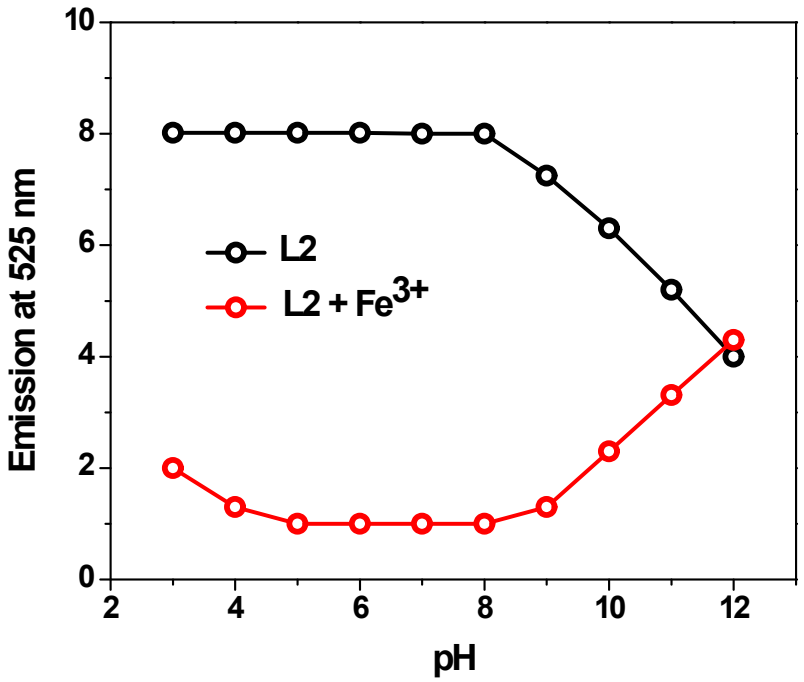

Figure S24. Effect of pH (3.0–12.0) on the emission intensity of chemosensor **L2** at 525 nm in the aqueous medium. The black and red circles respectively display emission intensity of chemosensor **L2** in the absence and presence of Fe^{3+} ion.

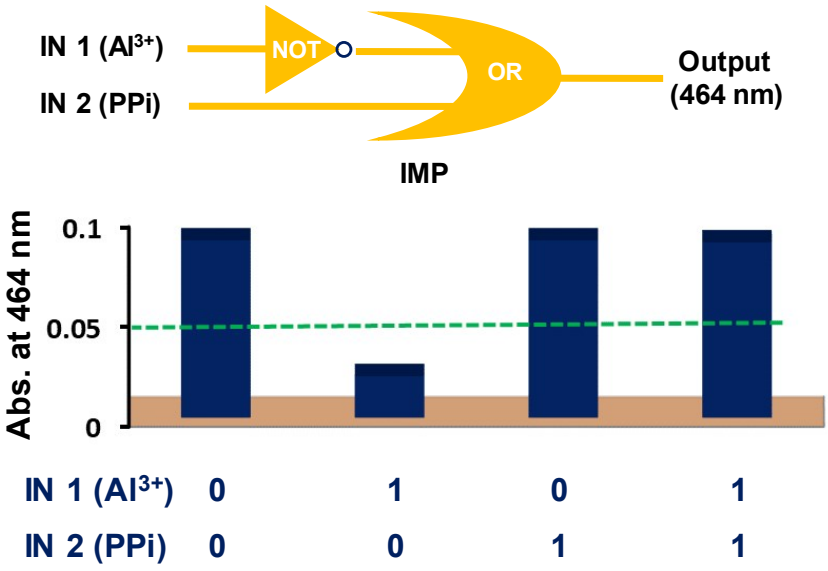

Figure S25. Absorbance outputs of chemosensor **L2** at 464 nm in presence of chemical inputs viz. IN 1 = Al^{3+} and IN 2 = PPi (blue bars) and the corresponding two-input combinational logic circuit (Threshold value is 0.05).

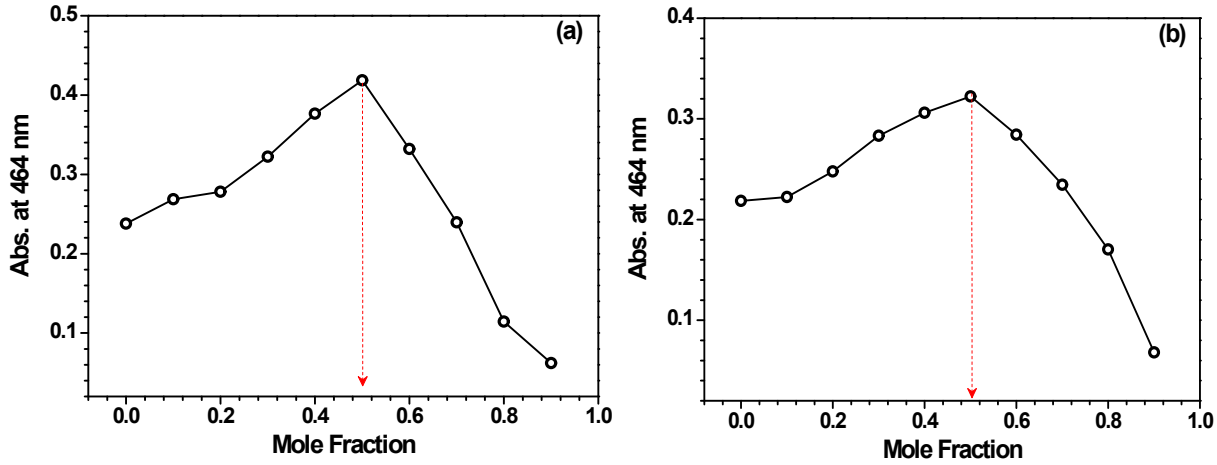

Figure S26. Job's plots for the detection of Al^{3+} ion by the chemosensors (a) **L1** and (b) **L2** in CH_3OH.

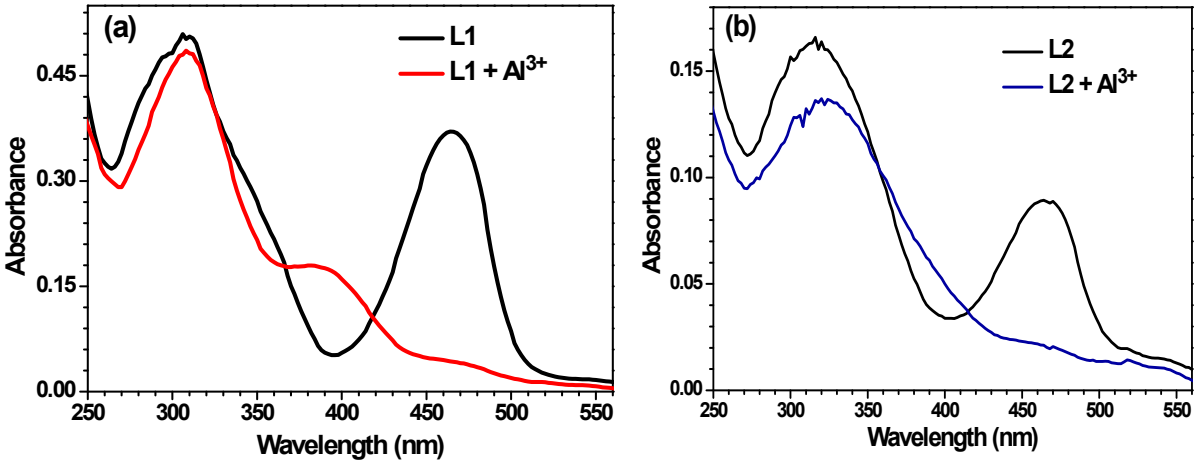

Figure S27. Change in the absorption spectra of chemosensors (a) **L1** and (b) **L2** in presence of two equivalents of Al^{3+} ion in CH_3OH.

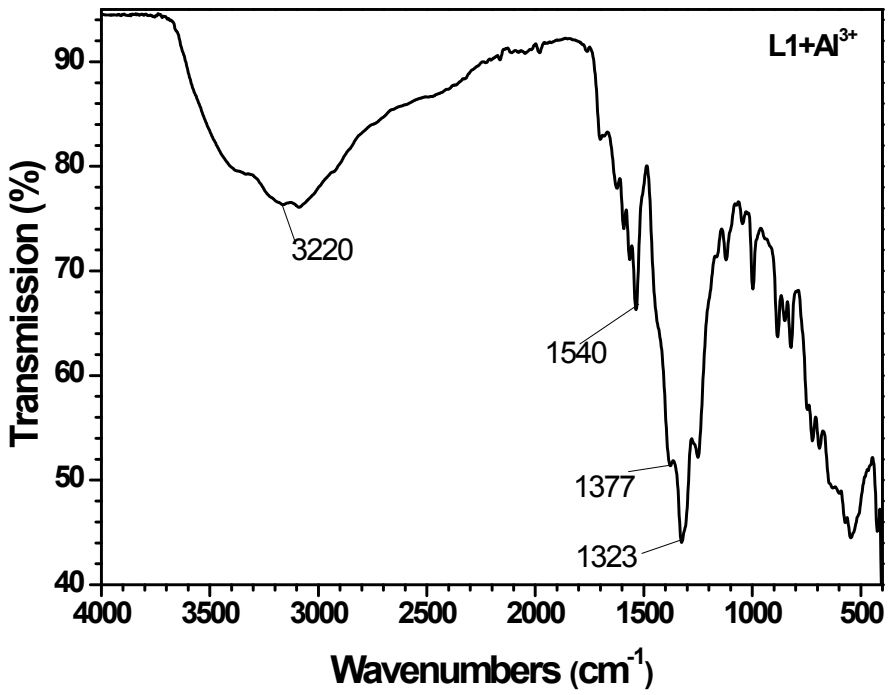

Figure S28. FTIR spectrum of isolated product [**L1–Al^{3+}**] from a reaction of chemosensor **L1** with Al^{3+} ion.

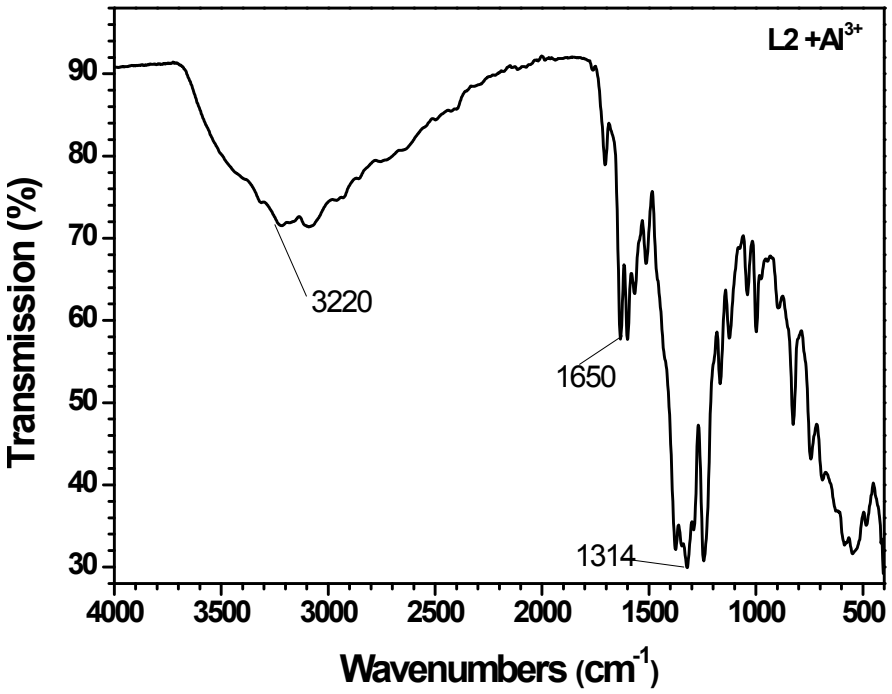

Figure S29. FTIR spectrum of isolated product [**L2–Al^{3+}**] from a reaction of chemosensor **L2** with Al^{3+} ion.

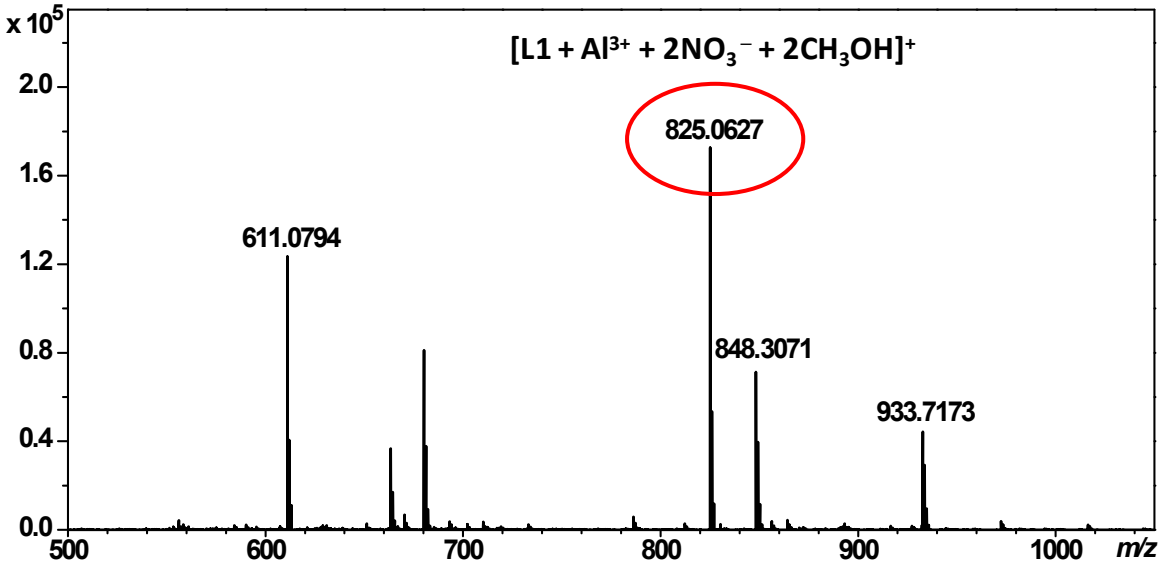

Figure S30. ESI$^+$-MS spectrum of isolated [**L1-Al^{3+}**] product in CH_3OH.

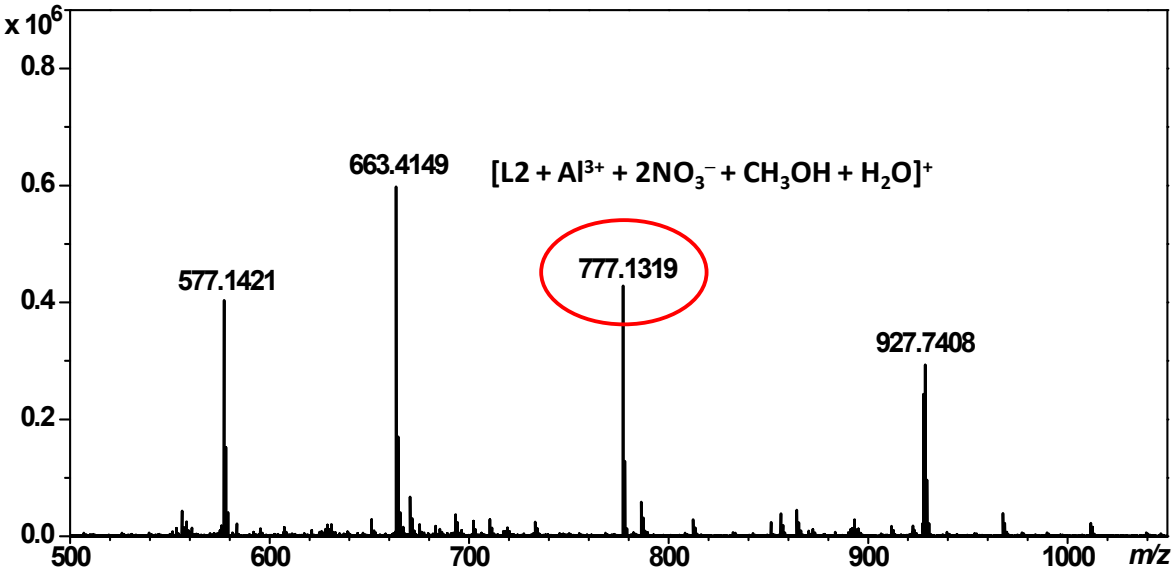

Figure S31. ESI$^+$-MS spectrum of isolated [**L2-Al^{3+}**] product in CH_3OH.

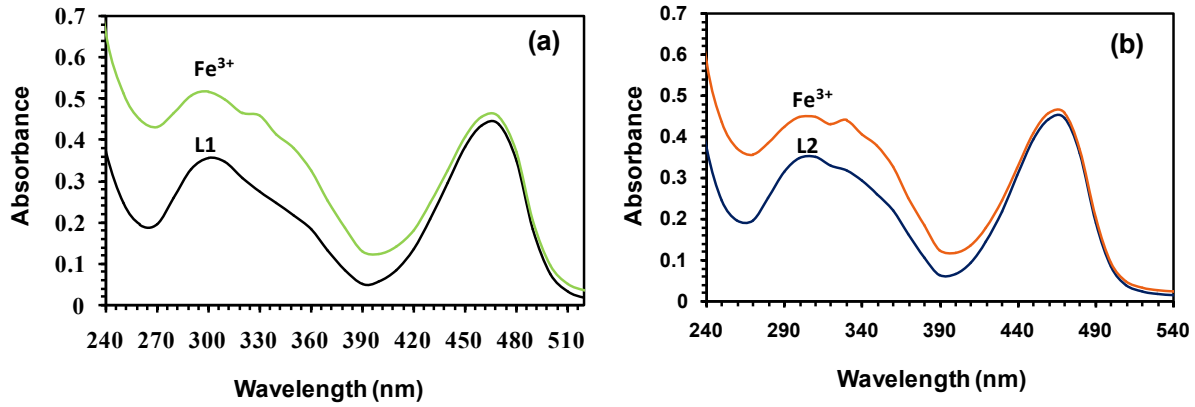

Figure S32. Change in the absorption spectra of chemosensors (a) **L1** and (b) **L2** in presence of two equivalents of Fe^{3+} ion in HEPES buffer.

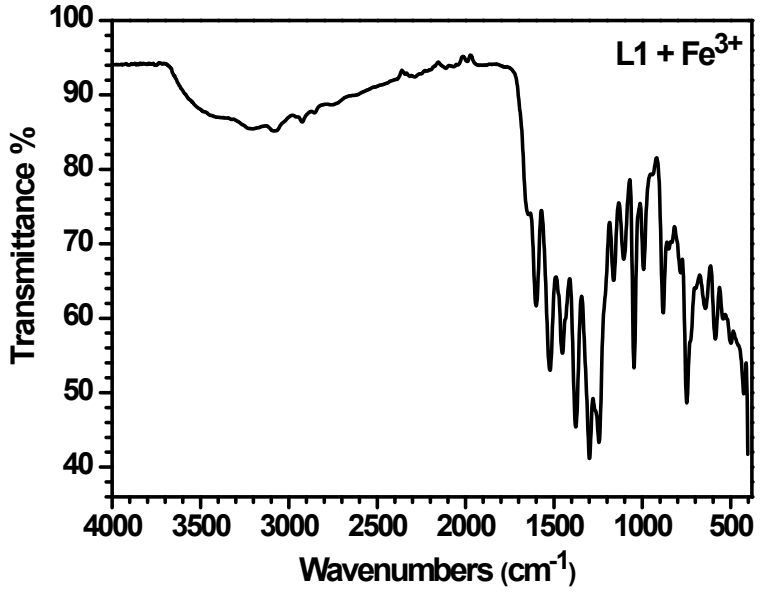

Figure S33. FTIR spectrum of isolated product [**L1–Fe^{3+}**] from a reaction of chemosensor **L1** with Fe^{3+} ion.

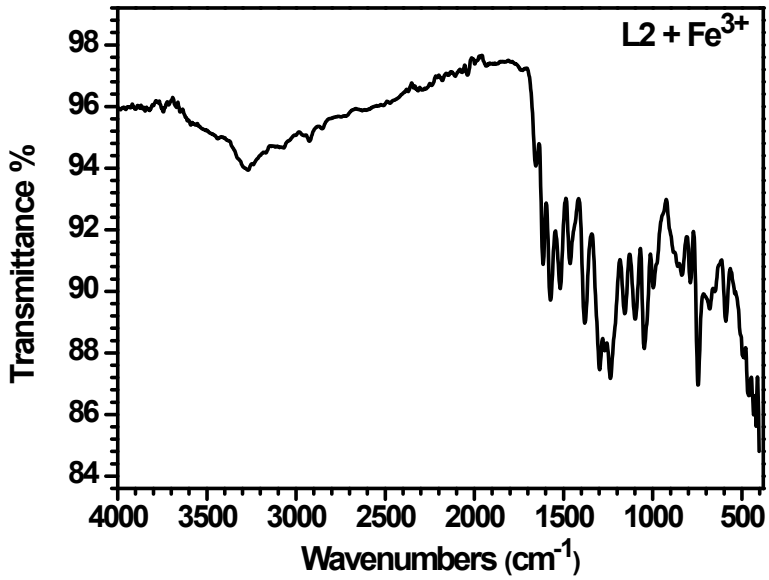

Figure S34. FTIR spectrum of isolated product [**L2–Fe**$^{3+}$] from a reaction of chemosensor **L2** with Fe^{3+} ion.

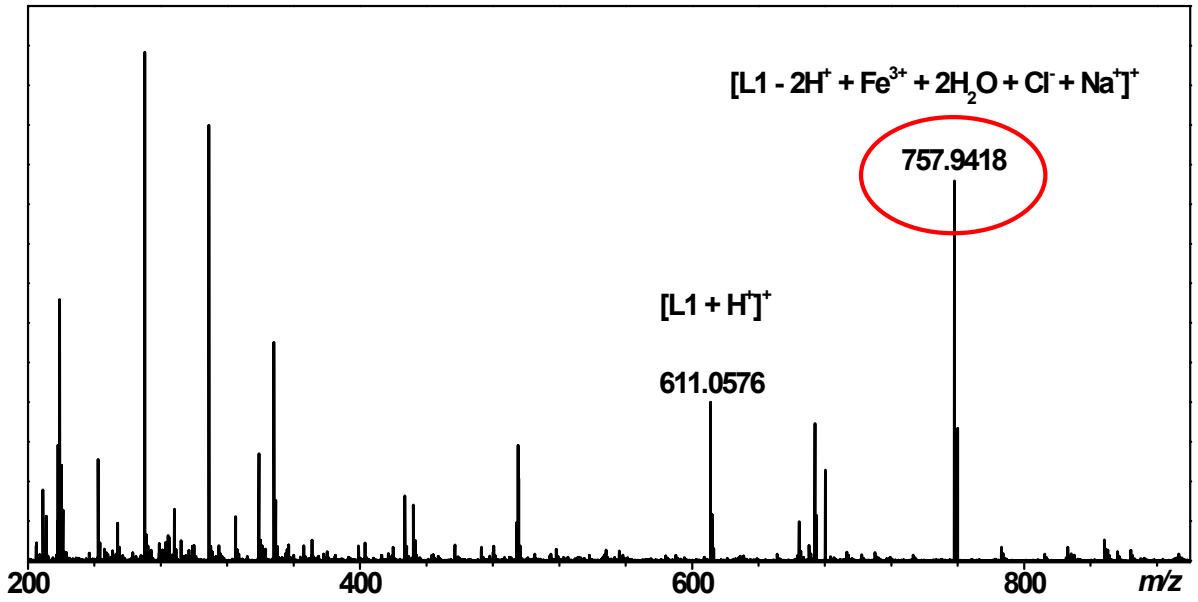

Figure S35. ESI^{+}-MS spectrum of isolated [**L2-Fe**$^{3+}$] product in H_2O.

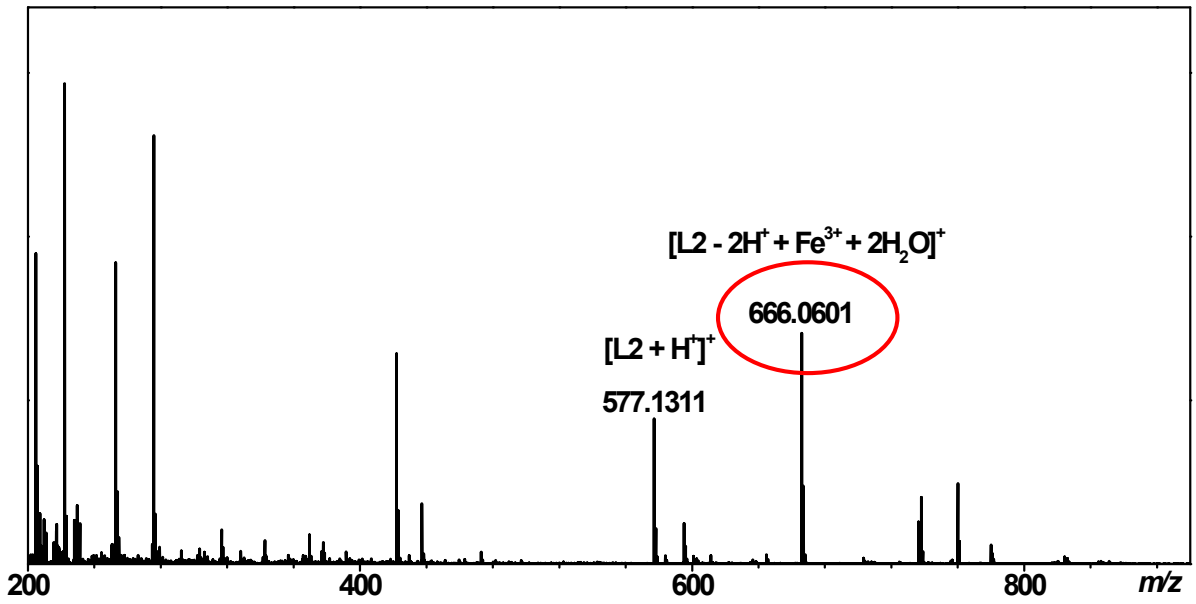

Figure S36. ESI$^+$-MS spectrum of isolated [**L2-Fe^{3+}**] product in H_2O.